Bull. Mater. Sci., Vol. 36, No. 2, April 2013, pp. 293–299. © Indian Academy of Sciences.

UV and visible light photodegradation effect on Fe–CNT/TiO_2 composite catalysts

ZHEN LI[1], JIN LIU[1,*], FENG-JUN ZHANG[1,2] and WON-CHUN OH[2,*]

[1]Anhui Key Laboratory of Advanced Building Materials, Anhui University of Architecture, Anhui Hefei 230 022, People's Republic of China

[2]Department of Advanced Materials & Engineering, Hanseo University, Seosan-si, Chungnam-do 356 706, Korea

MS received 31 March 2011; revised 28 September 2012

Abstract. **Using multi-walled carbon nanotube (CNT) as an one-dimensional support, we have succeeded in uniformly anchoring of TiO_2 and Fe nanoparticles at its surface. The as-prepared Fe–CNT/TiO_2 composite photocatalysts have been investigated by degrading methylene blue (MB) under UV and differently intensified visible light irradiation. The ability of CNT to store and shuttle electrons, and Fe nanoparticles demonstrate its capability to serve as a yield and transfer electrons on demand to separate h^+/e^- pairs. Moreover, the MB photodegradation increase with an increase of visible light intensity can be ascribed to the enhancement MB cationic radical. In addition, chemical oxygen demand (COD) of piggery waste and reduction efficiency of Cr (IV) was done at regular intervals, which gave a good idea about mineralization of wastewater.**

Keywords. **Fe–CNT/TiO_2 composites; photocatalytic activity; ultraviolet; visible light.**

1. Introduction

The photocatalytic activity of wide bandgap semiconductors has been the subject of numerous studies due to their ability to simultaneously harvest solar energy and drive chemical reactions via photoexcited charge carriers and activated electronic states (Fujishima and Honda 1972; Linsebigler *et al* 1995; Roy *et al* 2010). Among these materials, titania (TiO_2) is particularly noteworthy because of its robust performance, nontoxicity and chemical stability. Numerous photocatalytic applications for TiO_2 have been proposed including liquid- and gas-phase organic contaminant degradation and water photolysis (Fujishima and Honda 1972; Hoffmann *et al* 1995; Linsebigler *et al* 1995; Roy *et al* 2010). A popular pathway for enhancing photocatalytic activity is to form carbon nanotube (CNT)–TiO_2 composite photocatalysts (Serp *et al* 2003). CNT has been used as template or scaffold for the hybrid assembly of nanoparticles by keeping their morphology and structure even at high nanoparticle loadings (Fallmann *et al* 1999; Sun *et al* 2001; Jiang and Gao 2003). Thus, composites containing CNT are believed to provide many applications and exhibit cooperative or synergetic effects between TiO_2 and carbon phases (Kuo 2009; Zhang *et al* 2011). More recently, further enhancements to TiO_2 photocatalytic activity have been demonstrated by incorporating organic or inorganic species to CNT/TiO_2 composites and forming high photocatalytic activity of three phase's system (Han *et al* 2007; Oh *et al* 2010; Zhang *et al* 2010; Cong *et al* 2011; Wang and Zhou 2011). These organic or inorganic dopants have been proven to be an efficient root to alter photocatalytic activity under both UV and visible light. Among various dopants, Fe is the most frequent candidate, and the fact proves that the Fe-modified TiO_2 exhibits effective photocatalytic activity for degradation of organic pollutant under visible light irradiation (Yamashita *et al* 2003; Zhu *et al* 2006; Teoh *et al* 2007).

Incidentally, the photocatalytic activities of CNT/TiO_2 composites were usually tested by monitoring the decolourization of dyes as target substrates (Zhou *et al* 2010; Sampaio *et al* 2011; Yu *et al* 2011). However, a dye is not a suitable test substrate to evaluate the photocatalytic activity since the dye degradation is much affected by its adsorption affinity to carbon materials. In addition, dyes can be degraded through the sensitized path on the TiO_2, which complicates the mechanism of dye decolouration. Therefore, the previously reported photocatalytic activities of CNT/TiO_2 based on the dye decolouration are not very informative in understanding the role of CNT. Moreover, the organic or inorganic dopants in TiO_2 system did not explain effects of different energy photons.

Herein, we reported a simple synthesis route for Fe–CNT/TiO_2 composites using a sol–gel method and do not require any special equipment that other methods need. The photocatalytic activities are directly discussed by comparing CNT/TiO_2 and Fe–CNT/TiO_2 for degradation of insensitized piggery waste and MB under UV and different intensified visible light irradiations.

*Author for correspondence (liujin910@yeah.net; wc_oh@hanseo.ac.kr)

2. Experimental

2.1 *Materials*

As the support material, CNT were purchased from Carbon Nano-material Technology Co., Korea and used without further purification. *m*-chloroperbenzoic acid (MCPBA) was used as an oxidized reagent which purchased from Acros Organics, New Jersey, USA. Benzene (99·5%), which was used as an organic solvent, was purchased from Samchun Pure Chemical Co. Ltd., Korea. Titanium (IV) oxysulfate hydrate ($TiOSO_4 \times H_2O$ (TOS)) used as a titanium source for the preparation of the Fe/CNT–TiO_2 composite was purchased from Sigma–Aldrich Co. Ltd., Germany and $Fe(NO_3)_3 \cdot 9H_2O$ as the ferric source was purchased from Duksan Pure Chemical Co. Ltd., Korea. MB (analytical grade (≥99·99%)) was purchased from Duksan Pure Chemical Co. Ltd., Korea. Aqueous piggery waste was prepared by the adsorption filtration method with a porous activated carbon. Prior to adsorption, untreated pig urine and faeces (COD > 50000 mg/L) was filtered using membrane filtration with 2·2 μm size until faeces were no longer detected in the filtrate. The piggery waste was added to the porous activated carbon packed in a glass column and was then recovered from the column by elution with distilled water. The levels of the aqueous piggery waste can be reduced to 282 mg/L.

2.2 *Preparation of samples*

First, 2 g MCPBA was dissolved in 80 mL benzene. Then, 1 g CNT powder was put into the oxidizing agent solution, refluxed at 353 K for 6 h. Solid precipitates formed and were dried at 363 K. The oxidized CNT was added to 10 mL 0·1 M $Fe(NO_3)_3 \cdot 9H_2O$ solution and the mixtures were stirred for 24 h using a nonmagnetic stirrer at room temperature. After the heat treatment at 773 K, we obtained the Fe–CNT. On the other hand, 2 g TOS was dissolved in 200 mL of 5% concentration H_2O_2 to prepare the TOS solution. The Fe–CNT was put into the TOS solution prepared and then the mixed solution was stirred for 5 h in an air atmosphere. After stirring the solution transformed to gel state, and these gels were heat treated at 923 K for 1 h. Then, the Fe–CNT/TiO_2 composites were obtained. The procedure and nomenclatures of prepared samples are listed in table 1.

2.3 *Characteristics and investigations of samples*

The BET surface area by N_2 adsorption method was measured at 77 K using a BET analyser (Monosorb, USA). XRD (Shimadz XD-D1, Japan), the result was used to identify the crystallinity with CuKα radiation. SEM was used to observe the surface state and structure of Fe–CNT/TiO_2 composites using an electron microscope (JSM-5200, JEOL, Japan). TEM (JEOL, JEM-2010, Japan) at an acceleration voltage of 200 kV was used to investigate the size and distribution of the ferric and titanium deposited on the CNT surface. TEM specimens were prepared by placing a few drops of the sample solution on a carbon grid. EDX spectra were also obtained for determining the elemental information of CNT/TiO_2 and Fe–CNT/TiO_2 composites. UV-Vis absorption parameters for the MB solution degraded by CNT/TiO_2 and Fe–CNT/TiO_2 composites under UV lamp and different visible light irradiation were recorded using a Spectronic (Optizen Pop Mecasys Co. Ltd., Korea) spectrometer. Finally, the COD analyses were measured with a cell test spectrophotometer (PhotoLab S6, WTW, Germany) in accordance with standard cell test methods (Merck, Germany).

2.4 *Photocatalytic activity of samples*

The photocatalytic degradation was tested by Fe–CNT/TiO_2 composites powder and an aqueous solution of MB in a 100 mL glass container and then irradiation system with UV light at 365 nm and different intensity visible light (8, 35 and 60 W), respectively, which was used at a distance of 100 mm from the solution in darkness box. The Fe–CNT/TiO_2 composite powder (0·05 g) was suspended in 50 mL of MB solution with a concentration of $1{\cdot}0 \times 10^{-5}$ M. Then, the mixed solution was placed in the dark for atleast 2 h in order to establish an adsorption–desorption equilibrium, which was hereafter considered as the initial concentration (c_0) after dark adsorption. Experiments were then carried out under UV or under visible light. Solution was withdrawn regularly from the reactor at an order of 30, 60, 90 and 120 min; afterwards, 10 mL of solution was taken out and immediately centrifuged to separate any suspended solid. The clean transparent solution was analysed using a UV–Vis spectrophotometer.

A 0·2 mM solution of Cr (VI) was prepared by dissolving $K_2Cr_2O_7$ in water and pH of the solution was adjusted to

Table 1. Nomenclatures, BET surface area and EDX elemental microanalysis (wt%) of CNT, CNT/TiO_2 and Fe–CNT/TiO_2 composites.

Samples	Nomenclatures	S_{BET} (m^2/g)	Elements (wt%)			
			C	O	Ti	Fe
Pristine CNT		299	100	0	0	0
CNT + TOS	CT	185·32	48·55	22·87	22·54	0
CNT + $Fe(NO_3)_3$ (0·25 M) + TOS	FCT	147·5	46·76	24·43	21·46	7·35

2 using nitric acid. The experimental procedure was similar to degradation of MB and UV adsorption spectra were recorded to determine the final Cr (VI) concentration.

2.5 *COD test of samples*

The photocatalytic activities were also tested by measuring the degradation of piggery waste in aqueous media in a 100 mL glass container and then irradiation system with 20W UV light at 365 nm and different intensity visible light (8, 35 and 60 W), respectively, which was used at a distance of 100 mm from the solution in darkness box. The suspended sample (0·05 g) was kept at 0·005 g/mL. Then, the suspended solution was placed in the dark for atleast 2 h, in order to establish an adsorption–desorption equilibrium, which was hereafter considered as the initial concentration (c_0) after dark adsorption. Experiments were then carried out under irradiation system with stirring, which was measured at 150 min. The samples were withdrawn regularly from the reaction and dispersed powders were removed through a centrifuge. The clean transparent solutions were tested with a COD cell test photometer.

3. Results and discussion

The value of BET surface area of pristine CNT, CNT/TiO_2 and Fe–CNT/TiO_2 samples are presented in table 1 and are orderly denoted as CT and FCT, respectively. As the results of table 1 shown, the BET surface area of the as-received CNT is 299 m^2/g, while the BET surface area of CNT/TiO_2 decreases to 185·32 m^2/g, and achieves to 156·15 m^2/g after introduction of Fe. It can be evidently seen that there is a large change of the micropore size for CNT/TiO_2 and Fe–CNT/TiO_2 composites compared to corresponding CNT. Thus, both TiO_2 and Fe compounds can cause the variation of surface. The similar phenomena had also been observed in the references (Zhang *et al* 2008; Go *et al* 2009).

TEM images of CNT–TiO_2 and Fe/CNT–TiO_2 composites are shown in figure 1. The ordered microstructure of CNT–TiO_2 is kept unaffected partials of TiO_2 in figures 1(a and b) shows a few black dots, which corresponds to the Fe particles. There is an evidence of the formation of Fe-doped TiO_2 outside the pores in some segments, this is possibly associated with the formed crystalline of Fe and TiO_2, which is finely agreed with the XRD results. Both CNT–TiO_2 and Fe/CNT–TiO_2 composites should be a strong interphase structural effect between the carbon and TiO_2 phases, resulting in possible disappearance of CNT characteristic peaks in their XRD patterns due to a homogeneous dispersion of TiO_2 in CNT matrix.

Figure 2 shows the XRD pattern of the as-prepared CNT/TiO_2 and Fe–CNT/TiO_2 composites. The XRD results of Fe–CNT/TiO_2 composites illuminated that the CNT is coated with a mixed type of anatase and rutile TiO_2 particles. The major peaks are diffractions from (101), (004), (200) and (204) planes of anatase, and (110), (101), (111)

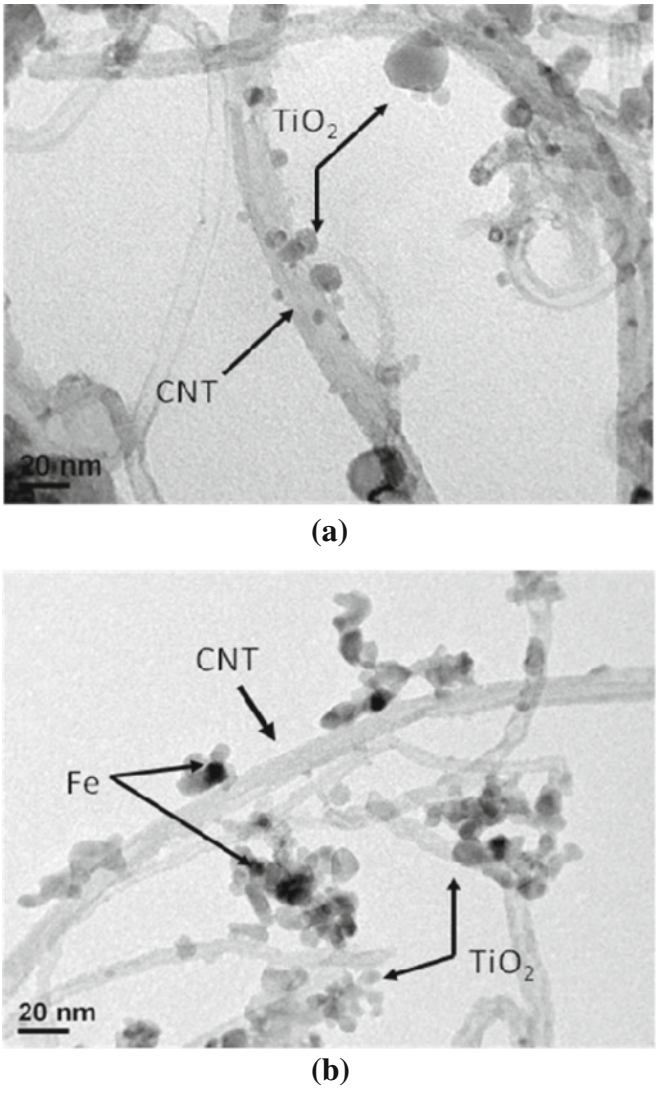

Figure 1. TEM micrograph of CNT/TiO_2 and Fe–CNT/TiO_2 composite catalyst: (**a**) CT and (**b**) FCT.

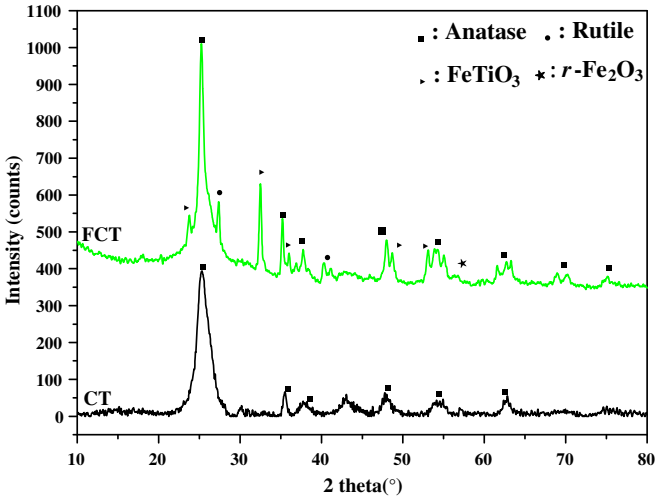

Figure 2. XRD patterns of powdered CNT/TiO_2 and Fe–CNT/TiO_2 composites.

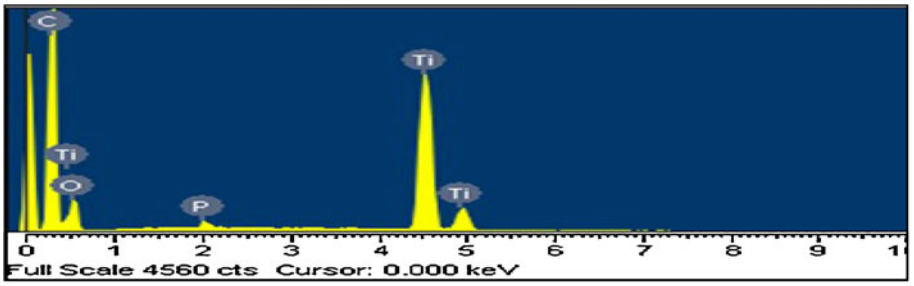

(a)

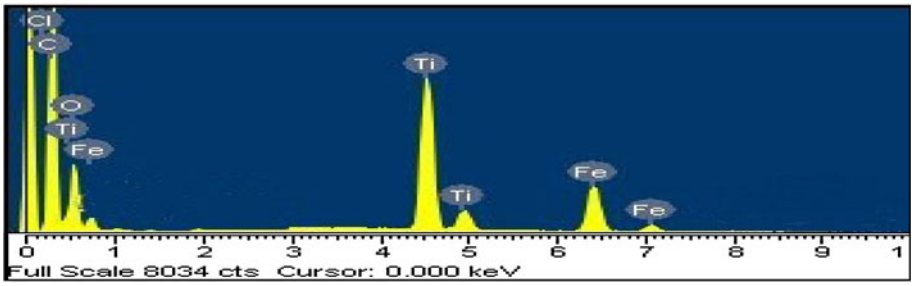

(b)

Figure 3. EDX elemental microanalysis of CNT/TiO_2 and $Fe–CNT/TiO_2$ composites: (**a**) CT and (**b**) FCT.

and (211) of rutile. The results indicate that the phase transition from TOS to the anatase and rutile phases took place at 923 K with formation of crystalline titania. However, the TiO_2 in CNT/TiO_2 composite only exhibits a typical single and clear anatase phase. The diffraction peak at $2\theta = 26{\cdot}5°$ can be well indexed as the 002 reflection of graphite, which could be noticed that the (101) anatase reflection overlaps the (002) reflection of carbon. Especially, pure maghemite (γ–Fe_2O_3) and uniform peaks of '$FeTiO_3$' could be obtained at $Fe–CNT/TiO_2$ composites, which indicate formation of the crystalline of Fe and TiO_2 due to reaction at high temperature.

Figure 3 shows the results of the EDX for CNT/TiO_2 and $Fe–CNT/TiO_2$ composites. These spectra show the presence of major peaks from the C, O and Ti elements. For the $Fe–CNT/TiO_2$ composites, we observe the peaks of the Fe element. The numerical contents for the various elements are also listed in table 1.

UV/Vis spectra of MB degradation by means of UV and visible light irradiation in the presence of $Fe–CNT/TiO_2$ composites are studied, respectively. The determined results are shown in figure 4. It could be found that the absorption peaks of MB solution at around 280 and 665 nm declined simultaneously along with UV irradiation in figure 4(a). These phenomena indicate that the degradation products of MB molecule possess same compound. Within 120 min UV irradiation all absorption peaks of MB solution decrease continuously, indicating that all MB in aqueous solution are degraded fully by electrons and holes reaction. Like UV irradiation condition, the UV/Vis spectra of the MB solution during visible light irradiation in the presence of $Fe–CNT/TiO_2$ composites are also determined in the wavelength range of 250–750 nm. The determined results are shown in figure 4(b). It could be also found that the absorption peak of MB solution at around 280 and 665 nm declined continuously along with visible light irradiation. The absorbance maxima (λ_{max}) values for the degraded MB products are remarkable similar to that of UV irradiation condition as a function of the degradation time against the $Fe–CNT/TiO_2$ composites, indicating that the degradation of MB under visible light irradiation also depends on generated electrons and holes.

To evaluate the adsorption ability of pure TiO_2, CNT/TiO_2 and $Fe–CNT/TiO_2$ composites, degradation of MB solution was run under dark condition which is graphically illustrated. From figure 5, it is clear that the degradation of MB on CNT/TiO_2 and $Fe–CNT/TiO_2$ composites is much higher than that of pure TiO_2, which correlates to a large surface area. However, the factors leading to the affected adsorption capacity should involve the change of the surface properties of the CNT and particle dispersions as TiO_2 and Fe. Therefore, compared to $CNT–TiO_2$ composite, the higher adsorption ability of the $Fe–CNT/TiO_2$ composites can be reasonably explained that the MB molecules are more close to a strip shape due to improving surface properties by the introduced Fe.

The photocatalytic degradation efficiency of MB under both UV light and visible light follows the order $Fe–CNT/TiO_2 > CNT/TiO_2 >$ pure TiO_2, as shown in figures 6 and 7. Clearly, the photocatalytic degradation efficiency of

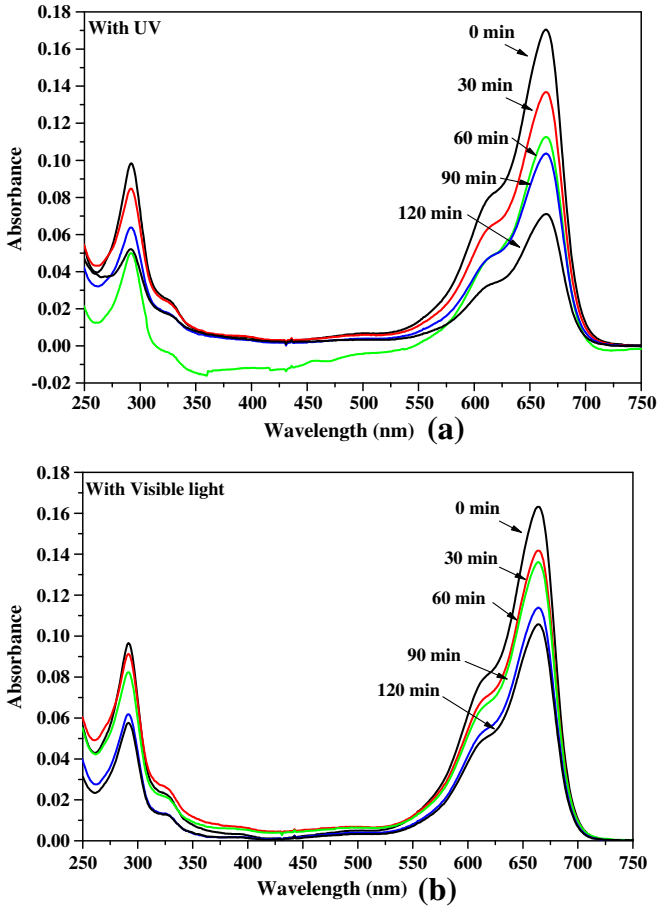

Figure 4. UV/Vis spectra of MB concentration against the Fe–CNT/TiO$_2$ composites under UV and visible light irradiation after photolysis as time function. (**a**) UV irradiation and (**b**) visible light irradiation.

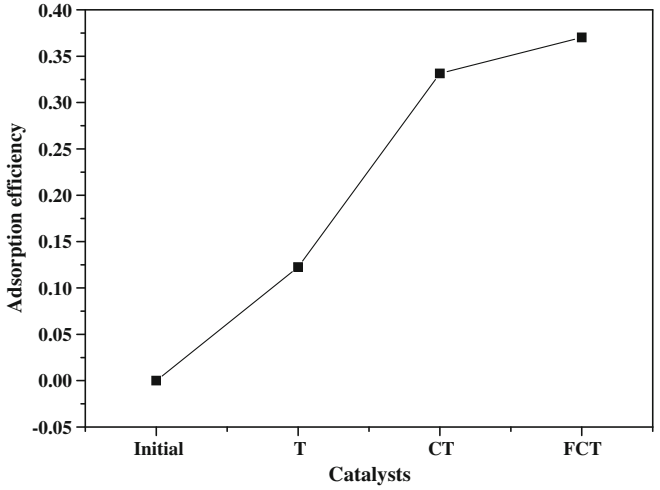

Figure 5. Adsorption capability of pure TiO$_2$, CNT/TiO$_2$ and Fe/CNT–TiO$_2$ composites for MB dyes under dark condition.

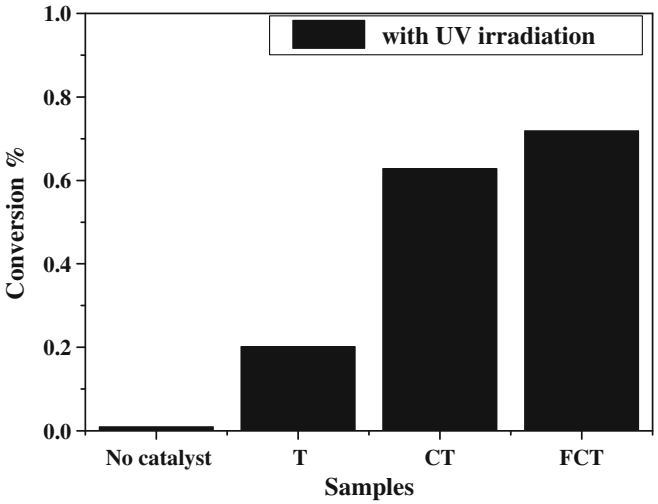

Figure 6. Photolysis conversion of MB under UV light irradiation for 120 min in presence of pure TiO$_2$, CNT/TiO$_2$ and Fe/CNT–TiO$_2$ composites.

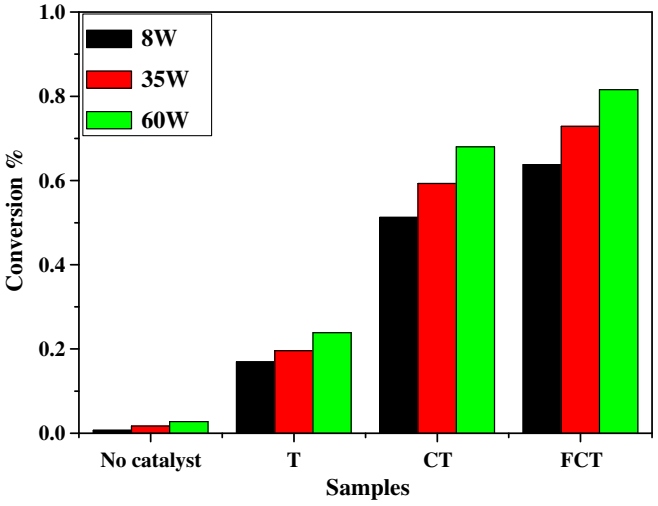

Figure 7. Effect of intensity visible light for pure TiO$_2$, CNT/TiO$_2$ and Fe–CNT/TiO$_2$ composites on photolysis conversion of MB at 120 min.

MB is negligible in the absence of photocatalyst, while the Fe–CNT/TiO$_2$ composites display a greater photocatalytic activity than CNT/TiO$_2$ and pure TiO$_2$, which can be considered that there are two main reasons. First, CNT enhances adsorptivity of MB molecules and electron–hole pairs lifetime (Chen *et al* 2009a,b). Second, deposited Fe further enhances above effects and provides a photo–Fenton reaction (Bauer *et al* 1999; Fullam *et al* 2000). To further increase the visible light intensity up to 60 W, indicating that MB molecules also act as a photosensitizer under high intensity light irradiation, resulting in more MB radicals formed on photocatalyst surface. It suggests that the photosensitized capability of MB molecules increases with an increase of light intensity.

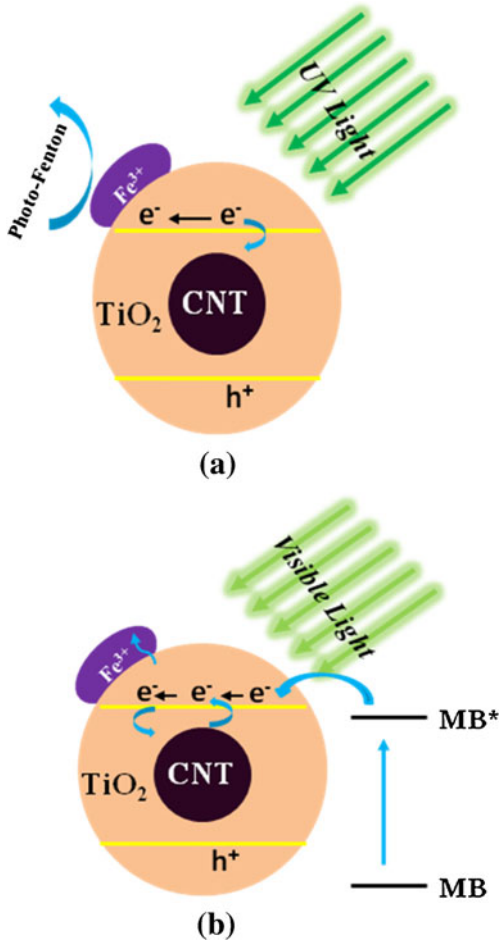

Figure 8. Reaction mechanism for MB photodegradation on Fe–CNT/TiO_2 composites.

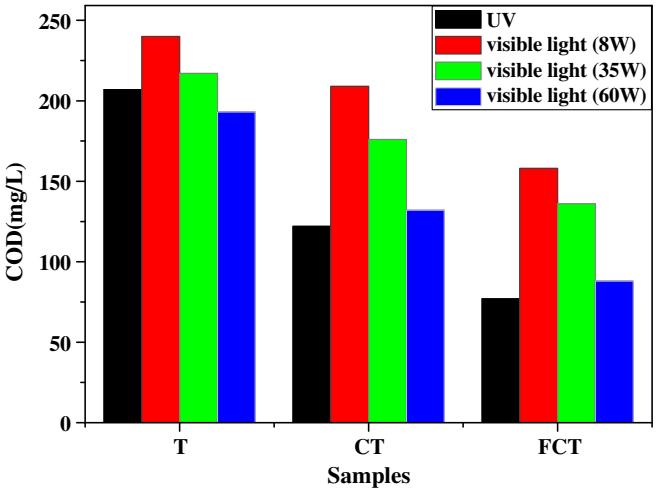

Figure 9. Results of COD removal efficiencies by pure TiO_2, CNT/TiO_2 and Fe–CNT/TiO_2 composites for piggery waste.

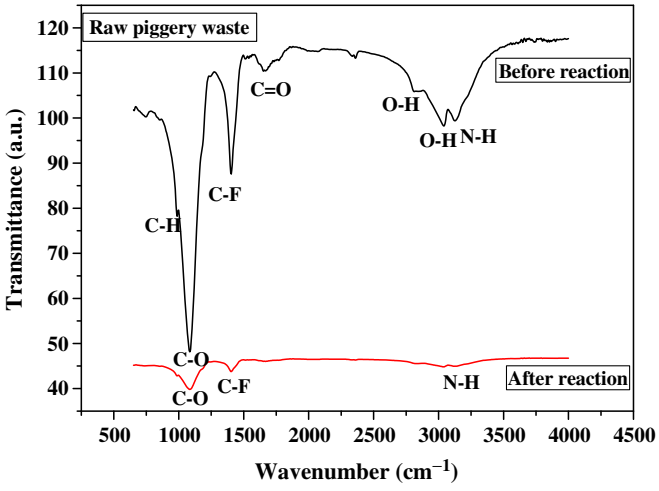

Figure 10. FT–IR spectra of piggery wastewater before and after reaction.

Figure 8 shows the possible photocatalytic pathways under UV and visible light irradiation for the MB photodegradation in Fe–CNT/TiO_2 composite. TiO_2 was first photoexcited to produce h^+ and e^- pair (1). The recombination rate of e^- and h^+ is more restrained as the electrons migrate to Fe and/or CNT, whereas the h^+ become trapped as the surface-bound $OH^{\cdot}$ radicals on oxidation of either the surface OH^- group and/or the surface H_2O molecules. Therefore, superoxide and hydroxyl radical production is enhanced.

The significantly enhanced photodegradation of MB in the Fe–CNT/TiO_2 under visible light irradiation may be ascribed to the cooperative roles of Fe deposits according to the mechanisms mentioned above as shown in figure 10(b). Due to self-photosensitization pathway for the MB photodegradation, this unexpected observation is most likely caused by photosensitized capability of MB molecules, since it has been accepted that the dye molecules can be excited by the visible light and inject electrons to the conduction band of TiO_2 (Li *et al* 2006).

Figure 9 presents changes of the chemical oxygen demand (COD) in the piggery wastewater as real wastewater. The COD parameter is defined as the mg O_2 consumed per litre of sample under UV and visible light irradiation. The average value of the initial COD of raw waste exceeded 282 mg/L. Similar with the experimental result on the MB degradation, the Fe–CNT/TiO_2 composite shows best COD removing abilities, and the COD removing efficiencies of which is as high as 75% under UV irradiation. Moreover, the varying tendencies of the MB degradation efficiencies do always keep in agreement with the COD removing efficiencies under visible light irradiation. For example, the Fe–CNT/TiO_2 appears to be the highest increase (~34·2, 37·3 and 54·4%) than that of CNT/TiO_2 (~12·9, 18·9 and 31·6%) compared to pure TiO_2 under different intensity visible light (8, 35 and 60 W), respectively. Thus, it should be noticed that the COD values can also be detected as compensation in the photodegradation experiments of dyes; new finding is that the high intensity visible light not only accelerates photosensitized capability of MB, but also benefits for photocatalytic activity of TiO_2 based photocatalysts. The FT–IR spectra of piggery wastewater before and after reaction are shown and the

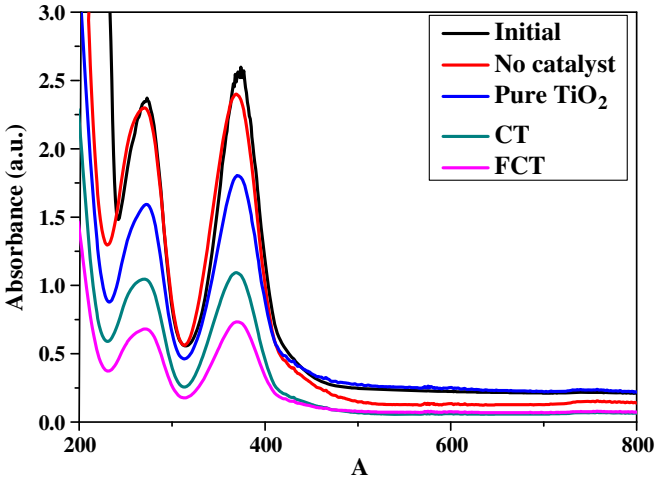

Figure 11. UV/Vis spectra of Cr (IV) concentration against pure TiO_2, CNT/TiO_2 and Fe–CNT/TiO_2 composites.

corresponding chemical bonds are inserted in figure 10. As shown in figure 10, it is clear that the corresponding chemical bonds are broken in the presence of photocatalysts.

To further verify the enhancement of photocatalytic activity, we also measure the photocatalytic properties of the Fe–CNT/TiO_2 composite in the reduction of Cr (IV) (0·2 mmol/L) under visible light irradiation (60 W). After 2 h irradiation, the UV/Vis spectra of Cr (IV) are shown in figure 11. With standard absorbance of Cr (IV) in 271 and 373 nm (Cho *et al* 2004), it is obvious that the Fe–CNT/TiO_2 composite has highest reduction efficiency when compared to pure TiO_2 and CNT/TiO_2.

Incidentally, the photocatalytic activities of nanocarbon semiconductor composites were usually tested by monitoring the decolourization of organic dyes as target substrate. However, a dye is not a suitable test substrate to evaluate the photocatalytic activity since the dye degradation is much affected by its adsorption affinity to nanocarbon. On the other hand, dyes can be degraded through the sensitized path of the semiconductor, which complicates the mechanism of dye decolourization.

4. Conclusions

In this study, we have investigated the photocatalytic performance of Fe–CNT/TiO_2 composite under UV and visible light irradiation. Compared to CNT/TiO_2 and pure TiO_2, the Fe–CNT/TiO_2 composite showed greater adsorption capability and photodegradation activity under UV and visible light irradiation. In addition, light intensity can influence photosensitized capability of MB molecules, even to TiO_2 based photocatalysts; high intensity light resulting in injecting more electrons to the conduction band of TiO_2. The Fe–CNT/TiO_2 composites also showed that it could be better effectuate to remove piggery wastewater and have highest reduction efficiency of Cr (IV), compared to pure TiO_2 and CNT/TiO_2. Overall results of the Fe–CNT/TiO_2 composites presented usability in UV and visible light system for water purification.

Acknowledgements

This work was financially supported by the Natural Science Foundation of China (No. 21171004) and the Natural Science Foundation of Anhui Province Education Department (KJ2011A064, KJ2011A070).

References

Bauer R, Waldner, Fallmann G H, Hager S, Klare M, Krutzler T, Malato S and Maletzky P 1999 *Catal. Today* **53** 131
Chen L C, Ho Y C, Guo W S, Huang C M and Pan T C 2009a *Electrochim. Acta* **54** 3884
Chen M L, Zhang F J and Oh W C 2009b *New Carbon Mater.* **24** 159
Cho Y M, Kyung H S and Choi W Y 2004 *Appl. Catal. B Environ.* **52** 23
Cong Y, Li X K, Qin Y, Dong Z J, Yuan G M, Cui Z W and Lai X J 2011 *Appl. Catal. B Environ.* **107** 128
Fallmann H, Krutzler T, Bauer R, Malato S and Blanco J 1999 *Catal. Today* **54** 309
Fujishima A and Honda K 1972 *Nature* **238** 37
Fullam S, Cottel D, Rensmo H and Fitzmaurice D 2000 *Adv. Mater.* **12** 1430
Go Y G, Zhang F J, Chen M L and Oh W C 2009 *J. Mater. Res.* **19** 142
Han T Y, Wu C F, Hsieh C and Vac T J 2007 *Sci. Technol.* **B25** 430
Hoffmann M R, Martin S C, Choi W Y and Bahnemann D W 1995 *Chem. Rev.* **95** 69
Jiang L Q and Gao L 2003 *Carbon* **41** 2923
Kuo C Y 2009 *J. Hazard. Mater.* **163** 239
Li Y Z, Kunitake T and Fujikawa S 2006 *J. Phys. Chem.* **B110** 13000
Linsebigler A L, Lu G and Yates J T 1995 *Chem. Rev.* **95** 735
Oh W C, Zhang F J and Chen M L 2010 *J. Ind. Eng. Chem.* **16** 312
Roy S C, Varghese O K, Paulose M and Grimes C A 2010 *ACS Nano* **4** 1259
Sampaio M J, Silva C G, Marques R R N, Silva A M T and Faria J L 2011 *Catal. Today* **161** 91
Serp P, Corrias M and Kalck P 2003 *Appl. Catal. A General* **253** 337
Sun YP, Huang W, Lin Y, Fu K, Kitaygorodskiy A, Riddle L A, Yu Y J and Carroll D L 2001 *Chem. Mater.* **13** 2864
Teoh W Y, Amal R, Mädler L and Pratsinis S E 2007 *Catal. Today* **120** 203
Wang S H and Zhou S Q 2011 *J. Hazard. Mater.* **185** 77
Yamashita H, Harada M, Misaka J, Takeuchi M, Neppolian B and Anpo M 2003 *Catal. Today* **84** 191
Yu J G, Fan J J and Cheng B 2011 *J. Power Source* **196** 7891
Zhang F J, Chen M L and Oh W C 2008 *Kor. J. Mater. Res.* **18** 583
Zhang F J, Chen M L and Oh W C 2010 *New Carbon Mater.* **25** 348
Zhang K, Zhang F J, Chen M L and Oh W C 2011 *Ultrason. Sonochem.* **18** 756
Zhou W, Pan K, Qu Y, Sun F F, Tian C G, Ren Z Y, Tian G H and Fu H G 2010 *Chemosphere* **81** 555
Zhu J F, Chen F, Zhang J L, Chen H J and Anpo M 2006 *J. Photochem. Photobiol. A Chem.* **180** 196